https://doi.org/10.1016/j.istruc.2021.09.056

Numerical investigation on the structural performance of octagonal hollow section columns

Hai-Xin LIU[a], Han FANG[b], Jiong-Yi ZHU[c] and Tak-Ming CHAN[a]*

[a] *Department of Civil and Environmental Engineering, The Hong Kong Polytechnic University, Kowloon, Hong Kong*

[b] *School of Civil, Environmental and Mining Engineering, The University of Adelaide, South Australia 5005, Australia*

[c] *Department of Civil Engineering, School of Mechanics and Engineering Science, Shanghai University, Shanghai 200444, China*

(* Corresponding author at: Department of Civil and Environmental Engineering, The Hong Kong Polytechnic University, Hong Kong, China. *E-mail address:* tak-ming.chan@polyu.edu.hk (T.-M. Chan).)

Abstract

This study is initiated by the increasing use of steel tubular members with octagonal hollow sections (OctHSs) in civil structures. Previous studies primarily focused on the local buckling behaviour of cold-formed steel OctHSs. However, investigations on the global buckling behaviour of OctHS long columns remain scarce. Thus, the main objective of this paper is to numerically investigate the structural performance of the OctHS columns. A finite element method (FEM) was developed for tubular columns and validated against relevant experimental results reported in the literature. Subsequently, a parametric study on 239 OctHS columns was carried out. The applicability of design methods outlined in Eurocode 3, ANSI/AISC 360-16 and ASCE/SEI 48-19 was evaluated. The evaluation shows that the design method in Eurocode 3 provides conservative predictions for the load-bearing capacity of OctHS columns, while the ANSI/AISC 360-16 design method was slightly unconservative for the strength predictions. The design method in ASCE/SEI 48-19 gave inaccurate predictions for the load-bearing capacity of the OctHS columns. Modifications to the design methods in ANSI/AISC 360 and ASCE/SEI 48-19 were proposed to improve the accuracy of

strength predictions and to obtain safe structural designs. The reliability of the design method in Eurocode 3 and the modified American design methods was assessed through the reliability analysis and found to satisfy the reliability requirements.

Keywords: Tubular column; Cold-formed octagonal hollow section; Finite element method; Design; Reliability analysis.

1. Introduction

Tubular sections, as an efficient cross-section type with merits of high resistance to torsional buckling, aesthetic appearance and acting as permanent formwork for concrete casting, are widely applied in structural engineering applications. Numerous research studies have been carried out over the last decades on the structural performance of rectangular, circular and elliptical steel hollow sections, covering the structures made of conventional strength steel and high strength steel with nominal yield strength up to 1100 MPa [1-8]. However, limited research has been conducted on the polygonal hollow sections. As one of the regular polygonal tubular hollow sections, the octagonal hollow sections have been applied in lighting masts, steel transmission pole structures, and single-pole supporting structures [9]. Compared with its rectangular counterparts, the octagonal cross-section has better local buckling resistance [10] and higher confinement effectiveness in concrete-filled steel tubes [11, 12]. Also, it can provide flat portions for the ease of connection construction, compared with circular cross-sections.

Recognizing these advantages, increasing experimental and numerical studies on the steel tubular structures with octagonal cross-sections have been performed in recent years [13-15]. Material properties and residual stress distributions, which are mainly dictated by the fabrication process, including welding and combination of welding and cold-forming, are of great significance to the performance of structural members. These properties of OctHS have been systematically investigated in experiments by Zhu et al. [16], Chen et al. [17] and Fang et al. [18], for the structures in different steel grades with nominal yield strength ranging from

355 MPa to 690 MPa. Based on the experimental research, models for predicting the material properties and residual stress patterns were also proposed in these studies. In addition to the investigations into material properties and residual stresses, research studies were also performed on the behaviour of OctHS stub columns made of steel in different grades. Gonçalves and Camotim [19] numerically investigated the elastic buckling behaviour of OctHS based on the Generalised Beam Theory (GBT). Chen et al. [20] and Fang et al. [21] conducted experimental and numerical investigations on the high strength steel OctHS stub columns. The results in these studies indicate that the cross-sectional classifications given in existing codes of practice including ANSI/AISC 360-16, ASCE/SEI 48-19, and Eurocode 3 are unsuitable for OctHSs under compression. Then Chen et al. [22] modified the cross-sectional classification limits outlined in current design codes based on the existing research results.

Although the behaviour of OctHS stub columns has been systematically investigated, limited attention has been paid to the OctHS column members that may experience the global buckling effect considered for their use in lighting poles and transmission towers. In order to generate safe structural designs, the structural performance of OctHS columns needs to be clearly understood. Therefore, the structural performance of cold-formed octagonal hollow section steel columns under concentric compression was numerically investigated in this paper. Firstly, the proposed FEM was validated against the existing experimental results of rectangular hollow section (RHS), square hollow section (SHS), circular hollow section (CHS) and OctHS stub columns. Following this validation, the proposed FEM was also validated against the structural performance of RHS, SHS and CHS long columns. Subsequently, extensive parametric studies on the structural performance of the OctHS columns were conducted using the validated FEM. The parametric studies cover the OctHS columns with steel grades from S355 to S690, and cross-section classifications from Class 1 to Class 4. Based on the results of parametric studies, the design methods given in Eurocode 3, ANSI/AISC 360-16 and ASCE/SEI 48-19 were evaluated for their applicability to the OctHS columns under compression. Modifications were suggested for the design methods in ANSI/AISC 360-16 and ASCE/SEI 48-19 to improve the accuracy of predictions. Reliability

analysis was also performed to assess the reliability of the design methods.

2. A finite element method for cold-formed hollow section columns

A FEM was developed for the numerical modelling on the structural performance of cold-formed hollow section columns through Geometrically and Materially Nonlinear Imperfect Analysis (GMNIA) using the finite element analysis software ABAQUS [23]. Experimental results for cold-formed steel columns with SHS, RHS, and CHS and nominal yield strength from 355MPa to 1100MPa, and with OctHS and nominal yield strength from 355MPa to 690 MPa [3, 8, 16, 20, 21, 24-27] were collated and used for validating the finite element method. These test data from experimental investigations in literature are summarized in Tables 1 and 2 using the nomenclature in Fig. 1. These previous studies provided experimental observations into the structural behaviour of cold-formed steel hollow section columns, which can be replicated by an appropriate finite element model.

2.1 Description of the finite element method

S4R shell element is adopted since it is suitable for the simulation of steel hollow section structures [1, 3, 20]. To accurately model the structures, measured geometrical dimensions and material properties were incorporated into the FE models. The engineering stress-strain curves obtained from the tensile coupon tests were converted to true stress-plastic strain curves using Eqs. (1) and (2), in which E_a is Modulus of elasticity, σ_{eng} and ε_{eng} represent the obtained engineering stress and the engineering strain respectively, σ_{true} denotes the converted true stress and ε_p is the converted logarithmic plastic strain.

$$\sigma_{true} = \sigma_{eng}(1+\varepsilon_{eng}) \tag{1}$$

$$\varepsilon_p = \ln(1+\varepsilon_{eng}) - \frac{\sigma_{true}}{E_a} \tag{2}$$

The cross-section of each structure with SHS, RHS and OctHS in the finite element model

was divided into different parts to distinguish the flat and corner portions since the material of the corner portion was deemed different from that in the flat portion due to the cold-forming process. The strength enhancement caused by cold-working was also found to be extended from the corner portion to the adjacent flat portion [3]. Therefore, the measured material properties of the corner region would also be assigned to the flat region that was adjacent to the corner. It is found in Ma et al. [3] and Chen et al. [22] that strengths prediction from FE models were in the best agreements with experimental results if the properties of the corner region were extended beyond to a width of $2t$ for RHS and SHS, or extended to a width of t for OctHS.

Residual stresses that existed in the cold-formed hollow sections can be attributed to the mechanical fabrication and uneven cooling process after welding. The residual stresses may cause reductions in resistance [17, 18, 28], and their effect on the structural performance of cold-formed hollow section structures has been investigated [3, 29, 30]. The bending residual stresses were considered to be released when the coupons were extracted from the cold-formed hollow section structures, and made the coupon slightly curved. During the subsequent tensile coupon test, the bending residual stresses were reintroduced, and the coupon returned to its flat state under the tensile load. Therefore, the effect of bending residual stress can be regarded as being inherently incorporated into the measured stress-strain relationships of the materials [31]. The measured longitudinal membrane residual stress was found to have an insignificant effect on the maximum compressive capacity of cold-formed steel columns [3, 4, 20]. Thus, the longitudinal membrane residual stresses of the cold-formed hollow section were not incorporated into the FE model, considering its relatively low magnitude compared to the yield strength and its negligible effect on the axially compressive capacity.

For the stub columns, all degrees of freedom of both ends of each structure were fully restrained except for the axial displacement at the loading end. As for the long columns, each end of the column was coupled with a reference point through kinematic coupling. The rotation about the bending axis was allowed at the reference points, while the displacement

was restrained except for the axial displacement at the loading end. The structural performance of the cold-formed hollow section columns was susceptible to local and global imperfections. In order to take into account the effect of geometric imperfections, the lowest eigenmode deformed shapes obtained through the separate eigenvalue buckling analysis, were scaled by the measured local and global imperfection amplitudes and assigned into the model.

2.2. Validation

The FE model described in the previous section was applied to model the cold-formed hollow section stub columns in Table 1 and the modelling results were compared with experimental results to validate the FE model. The FE predictions for load-bearing capacity are compared with the experimental results in Table 1 and good agreements were obtained. The mean value of the maximum load-bearing capacities obtained from FEM N_{FE} over the ultimate resistance obtained in experiments N_{Exp} and the corresponding coefficient of variation (COV) are 1.02 and 0.02, respectively. The load-end shortening curves obtained from the modelling are depicted in Fig. 2 in comparison with those results recorded in experiments. The curves from FE modelling also compared well with the experimental results, as shown in the figure.

Apart from the validation for the capability to simulate the behaviour of stub columns, the global buckling behaviour of cold-formed hollow section long columns were also mimicked by the proposed FEM. Experiments on cold-formed hollow section steel column members under concentric compression were performed in recent years to study their global buckling behaviour [24-27]. To validate the proposed FEM against the experimental results for long columns, the measured geometric dimensions, material stress-strain curves, global imperfection and local imperfection amplitude presented in the literature for the experimental investigations were also incorporated into the FEM. Since the local imperfection amplitude of cold-formed CHS columns was not reported in the literature, a predictive equation of local geometric imperfection from Meng and Gardner [32] was adopted and the value equalled $0.01(Dt)^{0.5}$. The information of validated cold-formed SHS, RHS and CHS long column tests was summarised in Table 2. Typical load-mid height deflection curves predicted for the

columns were depicted in Fig. 3 in comparison with those from experiments. It was observed from the figure that load-mid height deflection curves predicted in FE modelling were in good agreement with those from experiments. In addition, the comparison of maximum load from FEM with those from experiments was also made to examine the accuracy of the FEM. The mean value of the N_{FE}/N_{Exp} was 0.99, with a corresponding COV of 0.04, as shown in Table 2. Overall, for the cold-formed hollow section columns with different cross-sections, the proposed FEM can accurately replicate the structural performance.

3. Parametric studies

Having proved the suitability of the FEM for cold-formed hollow section columns, it is convinced that this method can be applied to cold-formed octagonal hollow section columns. To investigate the structural performance of the cold-formed OctHS columns under concentric compression, parametric studies were performed on the structures with a wider range of steel grades, cross-sectional sizes, and member slenderness. A mesh size of $B/10$ was chosen for the parametric studies through a mesh convergency study. The nominal edge lengths B of OctHS were 60mm and 80mm, while the thickness t was kept as a constant value as 3mm. An outer corner radius R_O of $3t$ was adopted based on the statistical evaluation of the cold-formed OctHS specimens in existing studies [16, 20, 33]. With the steel grades varied to achieve a range of cross-sectional slenderness, cross-sections considered in the parametric studies were classified as Class 1 to Class 4 sections. The column lengths L investigated herein were varied to obtain member slenderness $\overline{\lambda}$ ranging from 0.19 to 2.59. The geometric dimensions of cold-formed OctHSs studied in the parametric analysis are provided in Table 3.

The steel grades for OctHS columns in parametric studies were determined based on the grades for the OctHS members applied in structural applications such as transmission structures. The common steel grades used for the structures are summarised in Table 4. In order to cover the steel grade range applied in practice, the grades for the parametric studies are S355, S460 and S690 and material properties were derived using the stress-strain models proposed based on the material properties measured for cold-formed OctHS structures in

[16-18]. The modulus of elasticity E_a, yield strength f_y (0.2% proof strength $f_{0.2\%}$) ultimate strength f_u and strain at ultimate strength ε_u of input materials are listed in Table 5, and the engineering stress-strain curves of the materials are plotted in Fig. 4. The same strength enhancement arrangement for the corner region introduced in Section 2.1 was also applied. The boundary condition and the finite element model for a typical OctHS column are shown in Fig. 5.

Both local and global imperfections, in the respect form of the lowest eigenmode deformed shapes, were simultaneously scaled with the respective amplitudes and incorporated into the FE models. The typical lowest eigenmode deformed shapes are illustrated in Fig. 6. The amplitude for local imperfection was taken as $0.1t$ based on the suggestions provided by Zhu et al. [16]. This local imperfection amplitude was found to provide the best agreement between the FE predictions and the experimental results and was also used for the investigation and design of OctHS stub columns in compression [22]. As for the global imperfections, the amplitude was considered in a conservative manner and taken as $L/1000$. This $L/1000$ value for global imperfection amplitude was widely adopted in the design of cold-formed hollow column members [4, 34], and was also applied in the simulation for the global buckling behaviour of those structures, providing an accurate strength prediction.

Although the effect of longitudinal membrane residual stresses on the cold-formed SHS, RHS and CHS long columns were verified as negligible, their effect on the cold-formed OctHS long columns still needs to be examined. It is noteworthy that the residual stress patterns are directly dependent on the fabrication routes. Hence, a longitudinal membrane residual stresses distribution obtained from [16] for the S355 cold-formed OctHS column was explicitly assigned into the FE model to examine its effect on the structural performance of OctHS long columns. The assigned residual stress distribution on the modelled specimens is shown in Fig. 7, where the portion in red denotes the tensile residual stress caused by the cooling of the welding seam. It is worth noting that the column lengths were varied to study the effect of longitudinal membrane residual stress on columns with different member slenderness. The comparison between the maximum loads obtained from the models with longitudinal

membrane residual stresses incorporated N_{RS} and without considering those residual stresses $N_{W/ORS}$ is presented in Fig. 8. The differences were all less than 1%, revealing the negligible effect of longitudinal membrane residual stresses on cold-formed OctHS columns. Following aforesaid details of FEM, a total of 239 numerical models of cold-formed OctHS columns covering a wide range of parameters were generated. Key results of the numerical models were captured and employed for further study.

4. Evaluation and modification of current design guides

4.1. General

The numerical results generated from the parametric studies described in the previous section are used for evaluating the applicability of current design guides to the cold-formed OctHS columns. The design guides for steel structures, including European standards (EN 1993-1-1 [35] and EN 1993-1-12 [36]) and American standards (ANSI/AISC 360-16 [37] and ASCE/SEI 48-19 [38]) allow the design of steel columns with nominal yield strength up to 700MPa. The suitability of these design guides for predicting the load-bearing capacities for the cold-formed OctHS column was examined and discussed, and modifications on the American standards were proposed to improve the accuracy of the prediction for load-bearing capacity of cold-formed OctHS columns.

4.2. Eurocode 3 design method

In the late 90s, ECCS proposed an Ayrton-Perry type formula for the design of steel columns. This Ayrton-Perry type formula can provide accurate predictions for the load-bearing capacity of steel columns and was eventually adopted in the current Eurocode 3. As recommended in Eurocode 3, the load-bearing capacity of steel columns should be computed by Eqs. (3) - (6).

$$N_{EC3} = \frac{\chi A f_y}{\gamma_{M1}} \tag{3}$$

$$\chi = \frac{1}{\Phi + \sqrt{\Phi^2 - \bar{\lambda}^2}} \tag{4}$$

$$\Phi = 0.5\left[1 + \alpha(\bar{\lambda} - 0.2) + \bar{\lambda}^2\right] \tag{5}$$

$$\bar{\lambda} = \sqrt{\frac{Af_y}{N_{cr}}} \tag{6}$$

where A represents the gross cross-sectional area for Class 1 to 3 sections and effective cross-sectional area for Class 4 section, f_y is the average yield strength (weighted by area) equals $(f_{y,f}A_f + f_{y,c}A_c)/(A_f + A_c)$, taking into account the corner yield strength with strength enhancements, χ is the reduction factor, $\bar{\lambda}$ indicates the member slenderness, α denotes the imperfection factor, and N_{cr} is the elastic critical buckling load.

To evaluate the applicability of Eurocode 3 specifications for column design to cold-formed OctHS columns, the maximum load-bearing capacity obtained from parametric studies were normalised and plotted against the member slenderness in Fig. 9, while the Eurocode 3 column buckling curves "a_0", "a", "b", "c" and "d" are also shown in the same figure for comparison. According to the dimensions of cross-sections for OctHS columns in parametric studies, the numerical results were further divided into two series, namely O60×3 and O80×3 series to investigate the difference in structural performance between these two series. It can be seen in Fig. 9 that variations on the structural performance of the O80×3 series mainly occurred in the range of low member slenderness ($0.2< \bar{\lambda} \leq 0.4$), where the failure mode of columns was primarily dominated by the local buckling behaviour. The normalised buckling strengths of O80×3 series structures are lower than those of the O60×3 series structures with the same member slenderness. This observation is due to the larger B and B/t ratios of the O80×3 cross-sections with relatively lower local buckling resistance. In the range of intermediate slenderness ($0.4< \bar{\lambda} \leq 1.2$), the failure mode of columns is the interaction of local and global buckling, and the load-bearing capacity of columns was greatly affected by the varied stress-strain relationship of materials. S460 and S690 series columns have a higher normalised buckling strength than those of the S355 series, showing that the Eurocode 3 design method provides a more conservative strength prediction for the columns with higher

steel grades [30]. When the member slenderness of the column increased to be over 1.2, the structural behaviour of columns was primarily controlled by the elastic global buckling. As shown in Fig. 10, the column buckling curve "c" using an imperfection factor α as 0.49 which was originally provided for cold-formed CHS, SHS and RHS columns, lies closely under the data for the normalised buckling strengths, providing a lower bound for the strength predictions. Hence, the column curve "c" was deemed safe for its use in the design of cold-formed OctHS columns. The mean value of normalised buckling strength χ for columns with steel grade of S355, S460, S690 were 1.062, 1.149 and 1.146 respectively, with the corresponding COV of 0.011, 0.055 and 0.064, as shown in Table 6.

4.3. ANSI/AISC 360-16 design method

With developments of the column manufacturing process and design concept, American standard ANSI/AISC 360-16 provides a single column curve. This column buckling curve can be applied for steel columns with all types of manufacturing processes, cross-sections and steel grades up to 700MPa under axial compression. In order to obtain a consistent format with Eurocode's nomenclature, two-stage AISC column buckling resistance prediction equations were adjusted and given as Eq. (7). In the equation, f_{cr} represents the elastic critical buckling stress while r is the radius of gyration.

$$N_{AISC} = \begin{cases} (0.658^{\frac{f_y}{f_{cr}}}) f_y A & \text{for } \bar{\lambda} = \sqrt{\frac{Af_y}{N_{cr}}} \le \frac{4.71}{\pi} \\ (0.877) f_{cr} A & \text{for } \bar{\lambda} = \sqrt{\frac{Af_y}{N_{cr}}} > \frac{4.71}{\pi} \end{cases} \quad (7)$$

$$f_{cr} = \frac{\pi^2 E}{(\frac{L}{r})^2} \quad (8)$$

To evaluate the accuracy of strength predictions based on ANSI/AISC 360-16, the unfactored (ϕ=1.0) AISC column curve was plotted with the normalised buckling strength χ against the member slenderness, as shown in Fig. 11. As can be seen from the figure, the data points for

columns with S460 and S690 steel cluster around the AISC column curve, indicating that the AISC column curve generally yields accurate predictions for these cold-formed OctHS columns. As for the columns made of S355 steel, the AISC column curve provides unconservative strength predictions. Compared with the column curves from Eurocode 3, the AISC column curve matches much well with the tendency of the numerical data. The mean value and corresponding COV of the strength predictions based on ANSI/AISC 360-16 were 0.976 and 0.056, respectively.

The statistical evaluation shows that the AISC design method provides a slightly unconservative prediction for the capacity of the cold-formed OctHS steel columns. To improve the accuracy of the predictions, a modification to the column curve was generated. A regression analysis was performed to generate the best fit of the column curve with the normalised strengths for the columns based on parametric studies results. Subsequently, Eq. (9) was obtained. The results of parametric studies are plotted in Fig. 12 in comparison with the modified AISC column buckling curve. It is worth noting that the unconservative strength predictions for S355 OctHS columns will be eliminated if compared with the factored (ϕ=0.9) AISC column curve. The reliability of the proposed design method was also statistically examined in Section 5.

$$N_{\text{Mod}} = \begin{cases} (0.630^{\frac{f_y}{f_{cr}}}) f_y A & \text{for } \bar{\lambda} = \sqrt{\dfrac{A f_y}{N_{cr}}} \le \dfrac{4.71}{\pi} \\ (0.796) f_{cr} A & \text{for } \bar{\lambda} = \sqrt{\dfrac{A f_y}{N_{cr}}} > \dfrac{4.71}{\pi} \end{cases} \tag{9}$$

4.4 ASCE/SEI 48-19 design method

ASCE/SEI 48-19 provides specifications for the design of cold-formed steel tubular members for transmission pole structures. The ASCE/SEI 48-19 column strength prediction equation adopted a similar form to that in ANSI/AISC 360-16. To make a direct comparison, the design

equations of ASCE/SEI 48-19 were normalised and expressed as Eq. (10), conforming to the format of ANSI/AISC 360-16.

$$N_{\mathrm{ASCE}} = \begin{cases} (1-\dfrac{f_{\mathrm{y}}}{4f_{\mathrm{cr}}})f_{\mathrm{y}}A & \text{for } \bar{\lambda} = \sqrt{\dfrac{Af_{\mathrm{y}}}{N_{\mathrm{cr}}}} \le \sqrt{2} \\ f_{\mathrm{cr}}A & \text{for } \bar{\lambda} = \sqrt{\dfrac{Af_{\mathrm{y}}}{N_{\mathrm{cr}}}} > \sqrt{2} \end{cases} \tag{10}$$

ASCE/SEI 48-19 proposed a specific cross-sectional classification limit for polygonal hollow sections and used a permitted compressive stress concept to calculate the cross-sectional capacity of the slender polygonal cross-section. As can be observed in Fig. 13, the ASCE/SEI 48-19 design method overestimates the strength for the majority of OctHS columns investigated in the parametric studies. Regarding the predicted strength of OctHS columns in the relatively low slenderness range, the inaccurate strength predictions may be attributed to the lack of experimental data. For the OctHS columns with higher member slenderness, the direct adoption of Euler's column curve without incorporating the geometric imperfection effect is somewhat optimistic in predicting the strengths for those columns. Hence, a modification was also suggested to correct the problem by adopting the same design equation Eq. (9). The prediction accuracy of the modified ASCE design method using Eq. (9) was improved as indicated in Fig. 14, while the mean ratio of $N_{\mathrm{u}}/N_{\mathrm{ASCE}}$ was raised from 0.875 to 1.040, as shown in Table 7.

5. Reliability analysis

The reliability of design methods in Eurocode 3 and American specifications for OctHS columns under concentric compression was evaluated in line with the requirements and procedures stipulated in EN 1990 [39] and ANSI/AISC 360-16, respectively. Different statistical parameters adopted in the reliability analysis were described in the following sections.

5.1. EN 1990 method

A partial factor γ_{M1} = 1.00 was applied to the column buckling resistance design formulas of Eurocode 3 to achieve the specified safety level. To reduce the scatter of the prediction, the database were categorised into three sub-sets, namely S355, S460, and S690 series according to the steel yield strength, to obtain the corresponding correction factor *b*, while *b* can be obtained by the linear regression of the ultimate loads from parametric studies versus the theoretical resistance values plot, as shown in Fig. 15. The basic variables modulus of elasticity E_a, yield strength f_y, cross-sectional area A in the theoretical resistance model were varied and their variations can be taken into account through COV, V_{Ea}, V_{fy}, and V_A, in accordance with the prEN 1993-1-1:2020 [40], as summarised in Table 8. The cross-sectional area A of the OctHS column was computed by the product of edge length and thickness, for which the COV was 0.009 and 0.025 in prEN 1993-1-1:2020, respectively. Hence, the COV of area V_A for the OctHS column can be subsequently determined and equals 0.026.

To separate the dependence of basic variables E_a, f_y and A [4, 41], the design model for column buckling resistance can be modified as Eq. (11). Subsequently, the COV of the resistance function V_{rt} for each specimen can be obtained by Eq. (12). For the case of the limited number of tests, the design value r_d can be expressed as Eq. (13). Finally, the corrected partial factors γ_{M1}^* can be obtained by the least-squares best fit to the slope of $r_{n,i}$ versus $r_{d,i}$ data pair, as expressed in Eq. (15). K in Eq. (11) is a constant, independent of the basic variables, k_1, k_2, and k_3 are the coefficients computed for each specimen, varying with the member slenderness, as plotted in Fig. 16, t_p is the *p*-fractile of the Student t-distribution [42] (for v = n-1 degrees of freedom and the failure probability was adopted as 0.1% here), and α_{rt} and α_δ are the weighting factors for Q_{rt} and Q_δ, respectively.

$$N_{b,R} = g_{rt} = KE_a^{k_1} f_y^{k_2} A^{k_3} \tag{11}$$

$$V_{rt} = \sqrt{(k_1 V_{E_a})^2 + (k_2 V_{f_y})^2 + (k_3 V_A)^2} \tag{12}$$

$$r_d = b g_{rt}(\underline{X}_m)\exp(-k_{d,\infty}\alpha_{rt}Q_{rt} - k_{d,n}\alpha_\delta Q_\delta - 0.5Q^2) \tag{13}$$

$$k_{d,n} = -t_p\sqrt{1+\frac{1}{n}} \tag{14}$$

$$\gamma_{M1}{}^{*} = \frac{\sum_{i=1}^{n} r_{n,i} r_{d,i}}{\sum_{i=1}^{n} r_{d,i}^2} \tag{15}$$

The key statistical parameters and results of the reliability analysis are summarised in Table 6. $\gamma_{M1}{}^{*}$ were estimated as 0.992, 0.878 and 0.887 respectively for S355, S460 and S690 cold-formed OctHS columns, indicating that the current partial factor γ_{M1} as 1.00 can be safely incorporated into the theoretical resistance model. A recent stochastic numerical study conducted by Somodi and Kövesdi [43] reveals that the γ_{M1} of cold-formed SHS columns regarding the selection of curve "c" for steels with nominal yield strengths of 460MPa and 700MPa are 0.88 and 0.87 respectively, which are very close to those obtained for cold-formed octagonal columns. Therefore, the Eurocode 3 design formula of column buckling resistance using curve "c" is confirmed applicable to the design of cold-formed OctHS columns under concentric compression, within the required safety level.

5.2. AISC method

For the design methods of ANSI/AISC 360-16 and ASCE/SEI 48-19 and the proposed modified methods, reliability analysis in line with the recommended procedures in ANSI/AISC 360-16 was performed to examine their reliability. A resistance factor ϕ = 0.9 was proposed for the current probability-based LRFD design method to achieve an acceptable safety level and was further incorporated into the design methods. Under different loading circumstances, a basic load combination of 1.2 × DL + 1.6 × LL and a DL/LL ratio of 1/3 [44] were taken into consideration from the practical view. The reliability index β was computing using Eq. (16) and the design rule was deemed as reliable if the reliability index β was greater than 2.6.

$$\beta = \frac{\ln\left(\frac{R_n}{P_m M_m F_m}\right)}{Q_m} \Big/ \sqrt{V_P^2 + V_M^2 + V_F^2 + V_Q^2} \tag{16}$$

where R_n/Q_m is the ratio of the nominal resistance to the average load effect, P_m, M_m and F_m represent the average ratios of obtained load-bearing capacities to the predicted load-bearing capacities, the actual yield strength to the nominal yield strength and the actual section modulus to the nominal section modulus, and V_P, V_M, V_F and V_Q are the coefficients of variation for P_m, M_m, F_m and the average load effect, respectively.

Key parameters and results of reliability analyses are listed in Table 7 and Table 8. Of the results investigated, the reliability index β for original ANSI/AISC 360-16 and ASCE/SEI 48-19 design methods were 2.533 and 1.978, respectively, implying that an unsatisfying reliability level was acquired for the design methods in those codes. However, the reliability of design methods was greatly improved after the proposed modifications, as indicated by the reliability indexes of 2.799 and 2.790 for modified ANSI/AISC 360-16 and ASCE/SEI 48-19 design methods, respectively.

6. Conclusions

This paper presents a numerical investigation of the structural performance of octagonal hollow section steel columns. A finite element method for cold-formed hollow section columns was developed and validated against the existing experimental results. The validated FE model was subsequently applied to carry out comprehensive parametric studies. A total of 239 cold-formed OctHS columns, covering conventional to high strength steel grades (S355, S460 and S690), Class 1 to Class 4 cross-sections, and a wider range of member slenderness, were investigated in the parametric study. The generated numerical data were further employed to evaluate the applicability of the current design codes. On the basis of the evaluation and modification of the design methods from different standards, the following conclusions can be drawn:

- The design method of column buckling resistance outlined in Eurocode 3, using the column buckling curve “c”, is deemed applicable and provides a lower bound when predicting the buckling resistance of cold-formed OctHS steel columns.

- The strength predictions from ANSI/AISC 360-16 are slightly unconservative. The prediction accuracy can be improved with the modification proposed for the design formulas.
- The assessment of the design method in ASCE/SEI 48-19 reveals that this design method seemed to provide an inaccurate resistance prediction value for cold-formed OctHS columns. Recommendations to improve the accuracy have been proposed.
- Reliability analyses in line with the procedures stipulated in EN 1990 and ANSI/AISC 360-16 are finally conducted to examine the reliability of the design methods in Eurocode 3 and modified American specifications. The results indicate that the current partial factor γ_{M1} = 1.00 in Eurocode 3 and the resistance factor ϕ = 0.9 in American specifications can be safely adopted in the design of the cold-formed OctHS steel columns.

7. Acknowledgements

The research work presented in this paper was supported by the Research Grants Council of the Hong Kong Special Administrative Region, China (Project No. 15217119).

References

[1] T.M. Chan, L. Gardner, Compressive resistance of hot-rolled elliptical hollow sections, Engineering Structures 30(2) (2008) 522-532.

[2] M. Sun, J.A. Packer, Direct-formed and continuous-formed rectangular hollow sections — Comparison of static properties, Journal of Constructional Steel Research 92 (2014) 67-78.

[3] J.-L. Ma, T.-M. Chan, B. Young, Experimental investigation on stub-column behavior of cold-formed high-strength steel tubular sections, Journal of Structural Engineering 142(5) (2016) 04015174.

[4] X. Meng, L. Gardner, Behavior and Design of Normal- and High-Strength Steel SHS and RHS Columns, Journal of Structural Engineering 146(11) (2020) 04020227.

[5] X.-L. Zhao, Section capacity of very high strength (VHS) circular tubes under compression, Thin-Walled Structures 37(3) (2000) 223-240.

[6] H. Ban, G. Shi, Y. Shi, M.A. Bradford, Experimental investigation of the overall buckling behaviour of 960MPa high strength steel columns, Journal of Constructional Steel Research 88 (2013) 256-266.

[7] J. Wang, L. Gardner, Flexural Buckling of Hot-Finished High-Strength Steel SHS and RHS Columns, Journal of Structural Engineering 143(6) (2017) 04017028.

[8] J. Nseir, Development of a new design method for the cross-section capacity of steel hollow sections, Université de Liège, Liège, Belgique, 2015.

[9] S. Kalaga, P. Yenumula, Design of electrical transmission lines: structures and foundations, CRC Press2016.

[10] W. Naohiro, I. Kikuo, O. Tadayoshi, K. Yosuke, 05.11: Local buckling behavior of octagonal hollow cross-section member under axial compression or bending shear, ce/papers 1(2-3) (2017) 1116-1122.

[11] J.-Y. Zhu, T.-M. Chan, Experimental investigation on octagonal concrete filled steel stub columns under uniaxial compression, Journal of Constructional Steel Research 147 (2018) 457-467.

[12] H. Fang, T.-M. Chan, B. Young, Structural performance of concrete-filled cold-formed high-strength steel octagonal tubular stub columns, Engineering Structures 239 (2021).

[13] J.-Y. Zhu, T.-M. Chan, Experimental investigation on steel-tube-confined-concrete stub column with different cross-section shapes under uniaxial-compression, Journal of Constructional Steel Research 162 (2019).1

[14] J. Chen, T.-M. Chan, R.K.L. Su, J.M. Castro, Experimental assessment of the cyclic behaviour of concrete-filled steel tubular beam-columns with octagonal sections, Engineering Structures 180 (2019) 544-560.

[15] J. Chen, T.-M. Chan, Experimental assessment of the flexural behaviour of concrete-filled steel tubular beams with octagonal sections, Engineering Structures 199 (2019).

[16] J.-Y. Zhu, T.-M. Chan, B. Young, Cross-sectional capacity of octagonal tubular steel stub columns under uniaxial compression, Engineering Structures 184 (2019) 480-494.

[17] J. Chen, H. Liu, T.-M. Chan, Material properties and residual stresses of cold-formed octagonal hollow sections, Journal of Constructional Steel Research 170 (2020) 106078.

[18] H. Fang, T.-M. Chan, B. Young, Material properties and residual stresses of octagonal high strength steel hollow sections, Journal of Constructional Steel Research 148 (2018) 479-490.

[19] R. Gonçalves, D. Camotim, Elastic buckling of uniformly compressed thin-walled regular

519 polygonal tubes, Thin-Walled Structures 71 (2013) 35-45.
520 [20] J. Chen, J.-Y. Zhu, T.-M. Chan, Experimental and numerical investigation on stub column
521 behaviour of cold-formed octagonal hollow sections, Engineering Structures 214 (2020) 110669.
522 [21] H. Fang, T.-M. Chan, B. Young, Behavior of Octagonal High-Strength Steel Tubular Stub
523 Columns, Journal of Structural Engineering 145(12) (2019) 04019150.
524 [22] J. Chen, H. Fang, T.-M. Chan, Design of fixed-ended octagonal shaped steel hollow sections in
525 compression, Engineering Structures 228 (2021) 111520.
526 [23] ABAQUS, Dassault Systems, Waltham, MA, USA, 2019.
527 [24] B. Somodi, B. Kövesdi, Flexural buckling resistance of cold-formed HSS hollow section members,
528 Journal of Constructional Steel Research 128 (2017) 179-192.
529 [25] J.-L. Ma, T.-M. Chan, B. Young, Cold-formed high strength steel tubular beam-columns,
530 Engineering Structures 230 (2021) 111618.
531 [26] G. Shi, X. Jiang, W. Zhou, T.-M. Chan, Y. Zhang, Experimental study on column buckling of
532 420MPa high strength steel welded circular tubes, Journal of Constructional Steel Research 100 (2014)
533 71-81.
534 [27] F. Javidan, A. Heidarpour, X.-L. Zhao, J. Minkkinen, Application of high strength and ultra-high
535 strength steel tubes in long hybrid compressive members: Experimental and numerical investigation,
536 Thin-Walled Structures 102 (2016) 273-285.
537 [28] A. Su, Y. Sun, Y. Liang, O. Zhao, Material properties and membrane residual stresses of S690 high
538 strength steel welded I-sections after exposure to elevated temperatures, Thin-Walled Structures 152
539 (2020) 106723.
540 [29] R.B. Cruise, L. Gardner, Residual stress analysis of structural stainless steel sections, Journal of
541 Constructional Steel Research 64(3) (2008) 352-366.
542 [30] H. Fang, T.-M. Chan, B. Young, Structural performance of cold-formed high strength steel tubular
543 columns, Engineering Structures 177 (2018) 473-488.
544 [31] H.G. Rasmussen KJR, Design of cold-formed stainless steel tubular members. I:columns, Journal
545 of Structural Engineering 119(8) (1993) 2349–2367.
546 [32] X. Meng, L. Gardner, Cross-sectional behaviour of cold-formed high strength steel circular hollow
547 sections, Thin-Walled Structures 156 (2020) 106822.
548 [33] H. Fang, T.-M. Chan, B. Young, Experimental and Numerical Investigations of Octagonal
549 High-Strength Steel Tubular Stub Columns under Combined Compression and Bending, Journal of
550 Structural Engineering 147(1) (2021) 04020282.
551 [34] X. Meng, L. Gardner, A.J. Sadowski, J.M. Rotter, Elasto-plastic behaviour and design of
552 semi-compact circular hollow sections, Thin-Walled Structures 148 (2020) 106486.
553 [35] EN 1993-1-1:2005. Eurocode 3: Design of steel structures -Part 1-1: General rules and rules for
554 buildings, European Committee for Standardization (CEN) Brussels (2005).
555 [36] EN 1993-1-12:2007. Eurocode 3: Design of steel structures -Part 1-12: additional rules for the
556 extension of EN 1993 up to steel grades S700, European Committee for Standardization (CEN)
557 Brussels (2007).
558 [37] ANSI/AISC 360-16. Specification for structural steel buildings, American Institute of Steel
559 Construction (AISC) Chicago (2016).
560 [38] ASCE/SEI 48-19. Design of steel transmission pole structures, American Society of Civil
561 Engineers (ASCE) Reston, Virginia (2019).
562 [39] EN 1990:2002. Eurocode - Basis of structural design, European Committee for Standardization

(CEN) Brussels (2002).
[40] prEN 1993-1-1:2020. Eurocode 3: Design of steel structures -Part 1-1: General rules and rules for buildings, European Committee for Standardization (CEN) Brussels (2020).
[41] K.H. LAW, Instabilities in Structural Steel Elliptical Hollow Section Members, Imperial College London Department of Civil and Environmental Engineering (2010).
[42] M. Holicky, Reliability analysis for structural design, SUN MeDIA Stellenbosch2009.
[43] B. Kövesdi, B. Somodi, Buckling resistance of HSS box section columns part I: Stochastic numerical study, Journal of Constructional Steel Research 140 (2018) 1-10.
[44] ASCE/SEI 7-16. Minimum Design Loads and Associated Criteria for Buildings and Other Structures, American Society of Civil Engineers (ASCE) Reston, Virginia (2016).

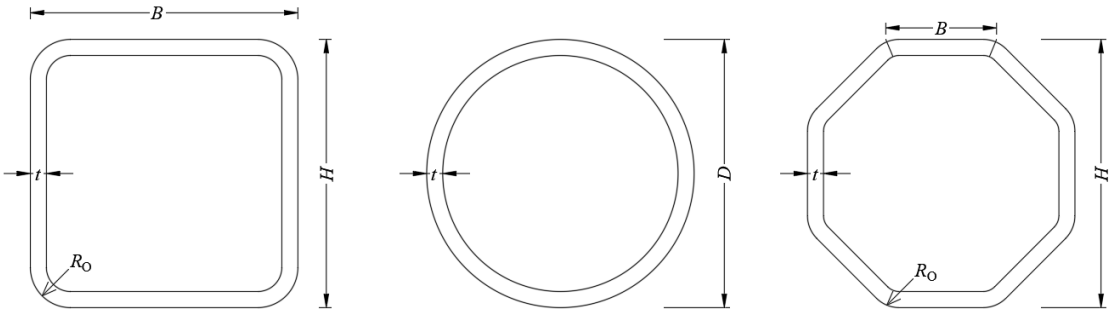

Fig. 1. Dimensions for different types of cold-formed hollow sections.

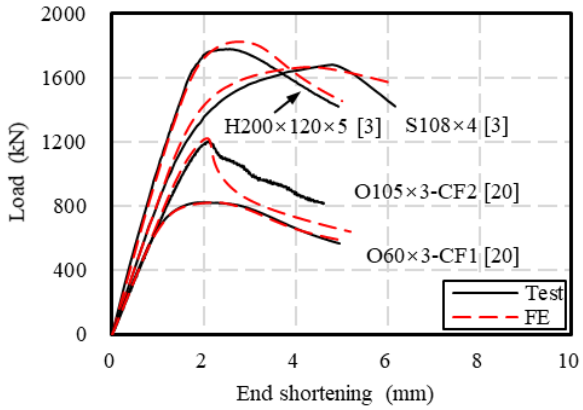

Fig. 2. Comparisons of load-end shortening curves of stub columns obtained from experiments and FE models.

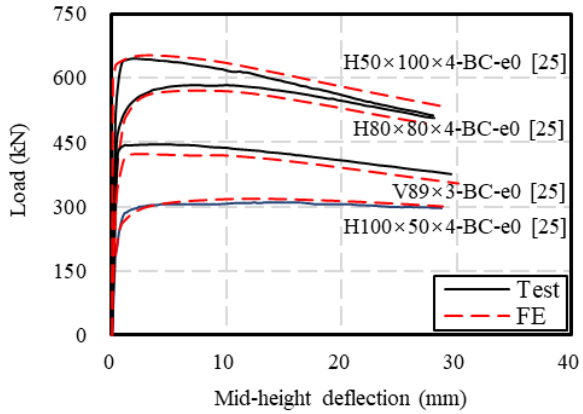

Fig. 3. Comparisons of load-mid height deflection curves of slender columns obtained from experiments and FE models.

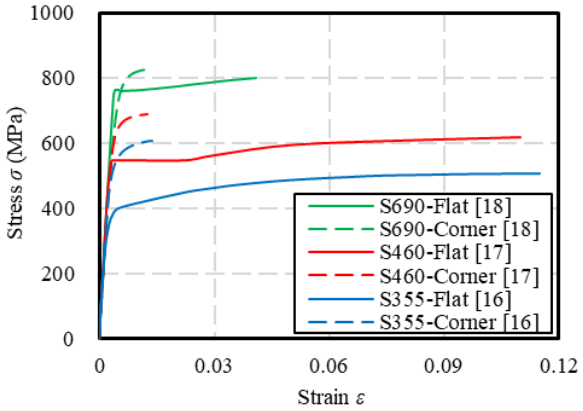

Fig. 4. Engineering stress-strain curves of input materials for parametric studies.

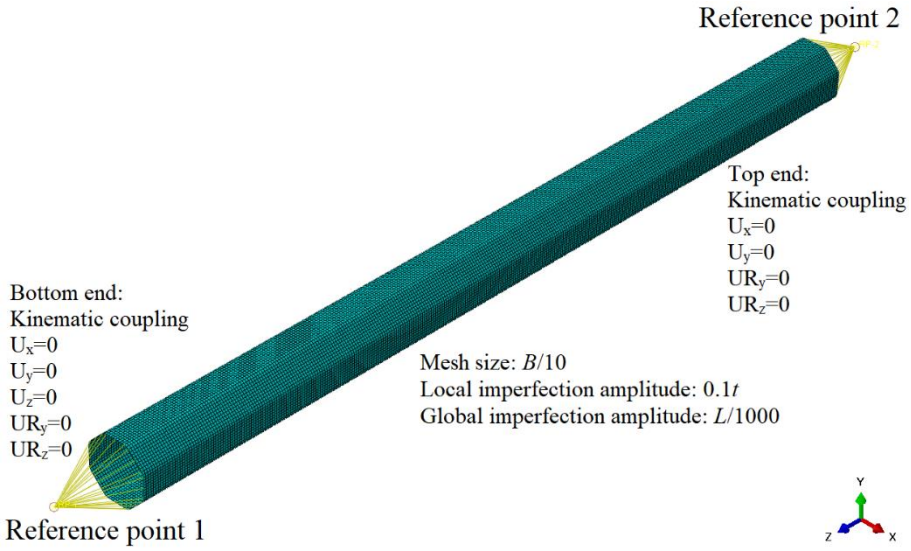

Fig. 5. The basic information of the modelled specimen.

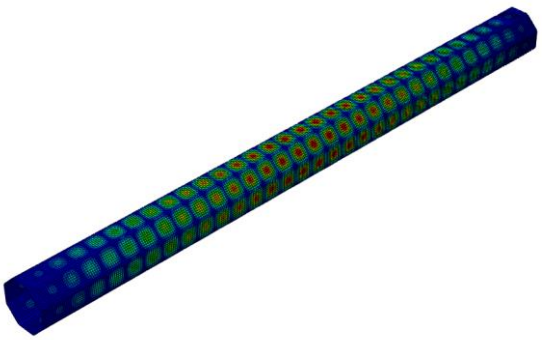

(a) Local imperfection profile.

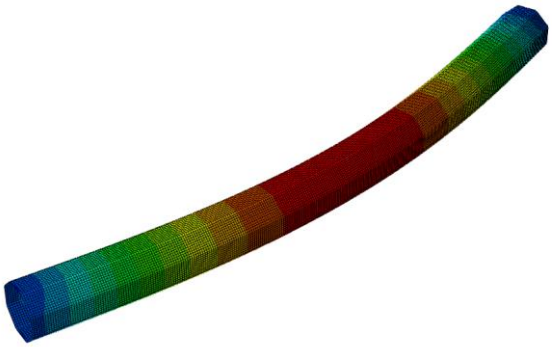

(b) Global imperfection profile.

Fig. 6. Typical deformed shapes of local and global imperfection.

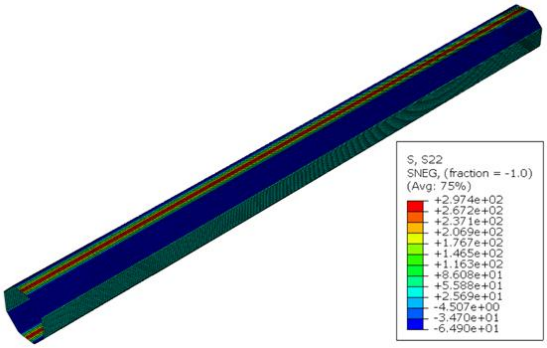

Fig. 7. The assigned residual stress distribution on the modelled specimens.

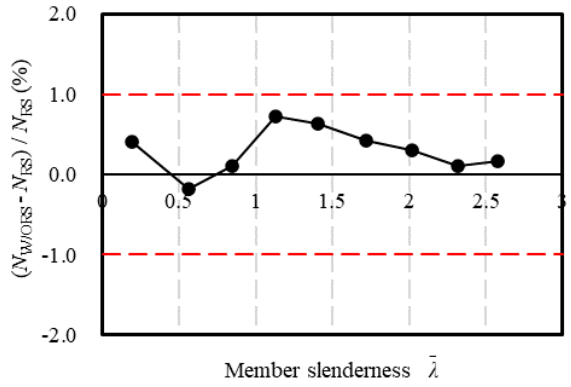

Fig. 8. The effect of longitudinal membrane residual stress on the load-bearing capacities.

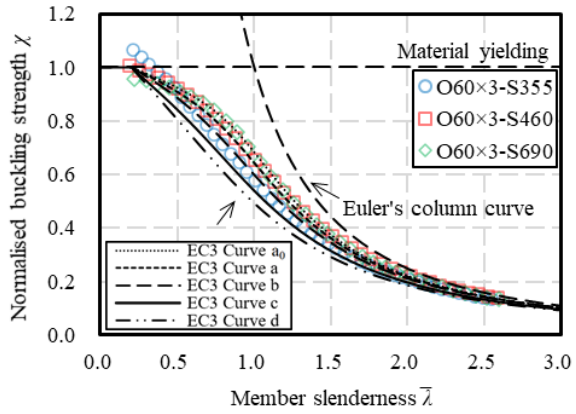

(a) O60×3 series.

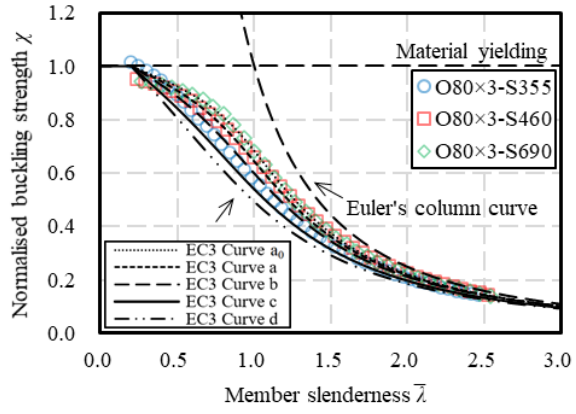

(b) O80×3 series.

Fig. 9. Comparisons of obtained results with different Eurocode 3 column buckling curves.

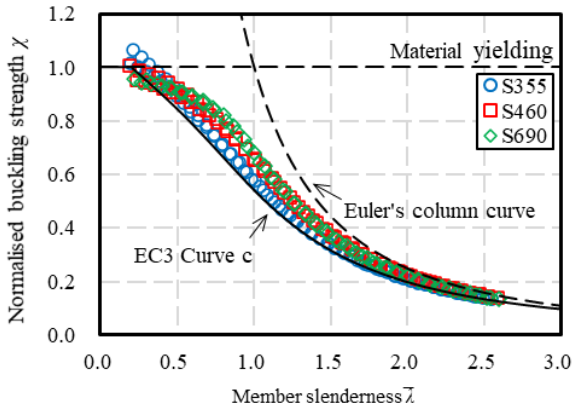

Fig. 10. Comparisons of all obtained results with Eurocode 3 column buckling curve "c".

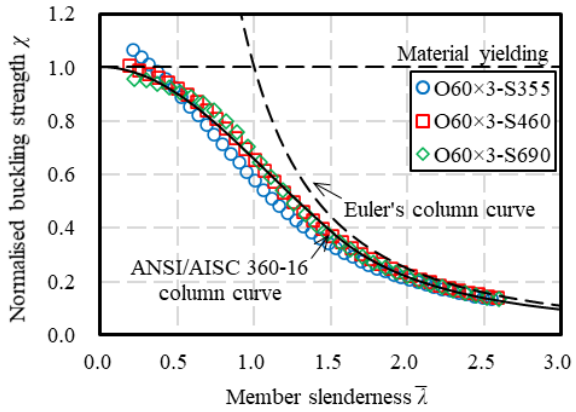

(a) O60×3 series.

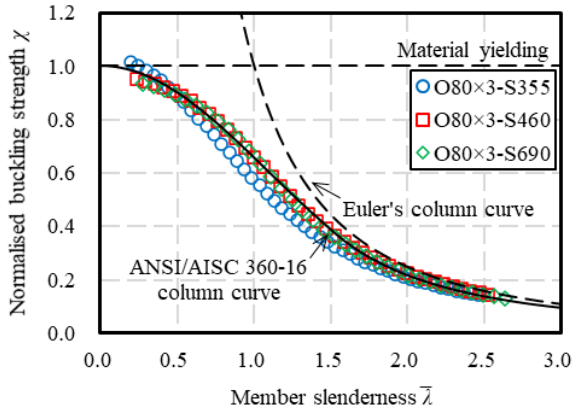

(b) O80×3 series.

Fig. 11. Comparisons of obtained results with ANSI/AISC 360-16 unfactored column curve.

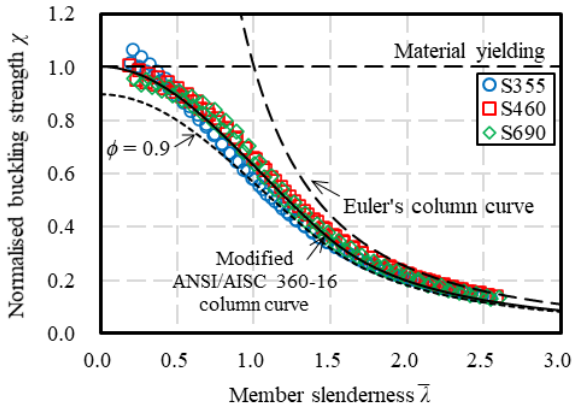

Fig. 12. Comparisons of obtained results with the modified ANSI/AISC 360-16 column curve.

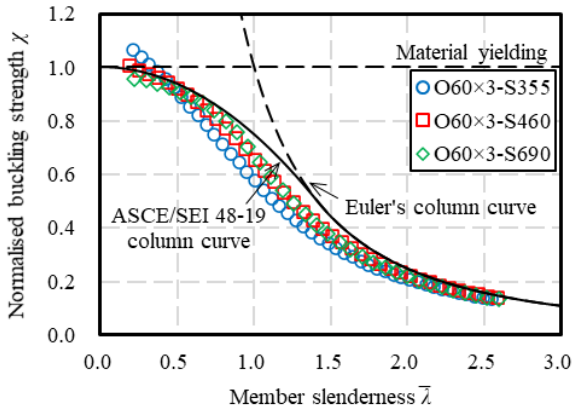

(a) O60×3 series.

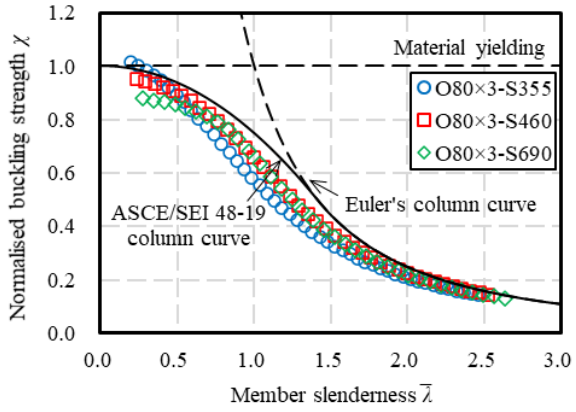

(b) O80×3 series.

Fig. 13. Comparisons of obtained results with ASCE/SEI 48-19 column curve.

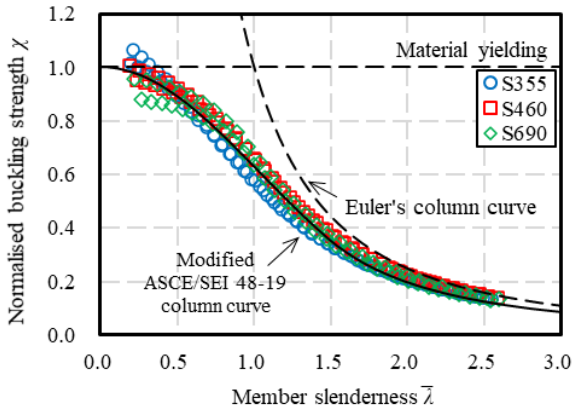

Fig. 14. Comparisons of obtained results with the modified ASCE/SEI 48-19 column curve.

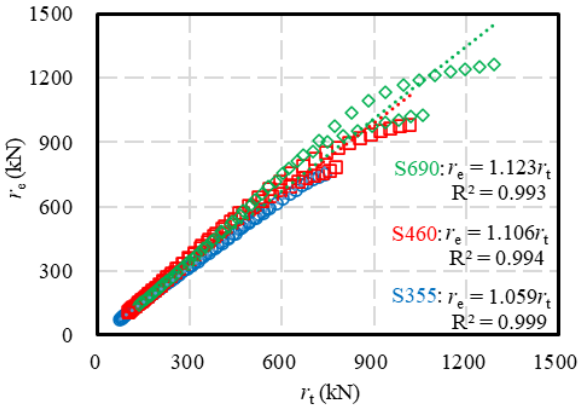

Fig. 15. r_e versus r_t data plot and corresponding linear regression fitting curves.

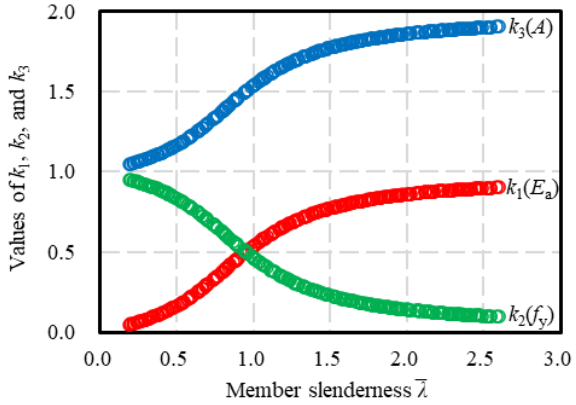

Fig. 16. The values of k_1, k_2 and k_3 against member slenderness.

Table 1. Cold-formed hollow section stub columns for FE model validation.

Cross-section	Specimens	Nominal steel grade	B (D)	H	t	R_o	Local imperfection	L	N_{Exp}	N_{FE}	N_{FE}/N_{Exp}
-	-	MPa	mm	mm	mm	mm	mm	mm	kN	kN	-
SHS/RHS [3, 8]	CF_200x200x6	355	199.50	199.00	6.58	13.20	0.33	600	1957	1989	1.02
	CF_200x100x4	355	200.50	100.28	3.69	7.40	0.18	600	761	791	1.04
	H100×100×4	700	100.50	100.20	3.92	8.50	0.11	300	1157	1150	0.99
	V100×100×4	900	100.30	100.40	3.97	11.50	0.30	300	1401	1372	0.98
	H200×120×5	700	200.30	120.50	4.94	13.00	0.18	565	1776	1821	1.03
CHS [3, 8]	CF_159x6.3	355	159.00	-	6.50	-	0.33	477	1800	1879	1.04
	V89×4	900	89.00	-	3.89	-	0.17	267	1171	1160	0.99
	S108×4	1100	108.20	-	3.90	-	0.14	324	1671	1664	1.00
	S133×4	1100	133.40	-	3.91	-	0.17	399	2018	2039	1.01
OctHS [16, 20, 21]	OctHS-1	355	73.73	178.00	5.55	16.60	0.56	695	1466	1514	1.03
	OctHS-2	355	73.73	178.00	5.54	16.60	0.55	695	1441	1514	1.05
	OctHS-3	355	73.73	178.00	5.53	16.60	0.55	695	1451	1514	1.04
	O60×3-CF1	460	61.10	147.50	3.03	10.00	0.30	431	822	823	1.00
	O105×3-CF2	460	106.00	255.90	3.04	10.00	0.30	757	1207	1224	1.01
	CF1-75×6a	690	74.10	179.00	6.20	20.60	0.62	499	2796	2856	1.02
	CF2-160×6a	690	159.70	385.60	6.02	20.40	0.60	1042	5489	5504	1.00
										Mean	1.02
										COV	0.02

Table 2. Cold-formed hollow section long columns for FE model validation.

Cross-section	Specimens	Nominal steel grade	B (D)	H	t	R_o	L	Local imperfection	Global imperfection	N_{Exp}	N_{FE}	N_{FE}/N_{Exp}
-	-	MPa	mm	mm	mm	mm	mm	mm	mm	kN	kN	-
SHS/RHS [24, 25]	CF4.2-R100 × 3_3B	420	100.25	100.45	3.23	6	2799	0.07	2.79	334	327	0.98
	H80×80×4-BC-e0	700	80.30	80.10	3.94	9.50	1655	0.19	0.43	582	568	0.98
	H100×50×4-BC-e0	700	100.20	50.60	3.97	8.50	1655	0.25	0.26	307	318	1.04
	H50×100×4-BC-e0	700	50.30	100.20	3.98	8.50	1655	0.25	0.03	642	653	1.02
CHS [25, 26, 27]	D420-20-2	420	275.00	-	6.01	-	1889	0.41	2.77	2173	2185	1.01
	V89×3-BC-e0	900	89.00	-	2.93	-	1655	0.18	0.17	444	415	0.93
	S-HST2	690	76.10	-	3.20	-	1400	0.16	1.4	368	360	0.98
	S-UHST2	1200	76.10	-	3.20	-	1400	0.16	1.4	584	596	0.96
											Mean	0.99
											COV	0.04

Table 3. Geometric dimensions of cold-formed OctHS columns in parametric studies.

Cross-section	Steel grade	B	H	t	R_O	L	Member slenderness
-	-	mm	mm	mm	mm	mm	-
O60×3	355	60.06	145.00	3.00	9.00	800-9600	0.21-2.54
O60×3	460	60.06	145.00	3.00	9.00	600-8200	0.19-2.59
O60×3	690	60.06	145.00	3.00	9.00	600-7000	0.22-2.59
O80×3	355	79.94	193.00	3.00	9.00	1000-12500	0.20-2.47
O80×3	460	79.94	193.00	3.00	9.00	1000-10750	0.24-2.53
O80×3	690	79.94	193.00	3.00	9.00	1000-9500	0.27-2.54

Table 4. The summarised yield strengths of commonly used structural steels in transmission structures [9].

Region	Yield strength f_y
-	MPa
U.S.	228 MPa - 448 MPa
Europe	235 MPa - 440 MPa
Canada	300 MPa - 400 MPa
Australia	250 MPa - 450 MPa
India	225 MPa - 352 MPa

Table 5. Summary of input material properties for parametric studies.

Steel grade	E_a	f_y	f_u	ε_u
-	GPa	MPa	MPa	%
S355-Flat, Zhu et al. [16]	213	379	503	10.1
S355-Corner, Zhu et al. [16]	214	548	596	1.3
S460-Flat, Chen et al. [17]	210	541	623	10.8
S460-Corner, Chen et al. [17]	201	655	690	1.2
S690-Flat, Fang et al. [18]	210	762	802	4.1
S690-Corner, Fang et al. [18]	191	775	825	1.2

Table 6. Results of the reliability analysis for Eurocode 3 design method.

Steel grade	Mean	COV	b	n	$k_{d,n}$	V_δ	γ_{M1}*
S355	1.062	0.011	1.059	92	3.131	0.011	0.992
S460	1.149	0.055	1.106	79	3.131	0.056	0.878
S690	1.146	0.064	1.123	68	3.131	0.065	0.887

Table 7. Results of reliability analysis for design methods of American specifications.

Design method	ϕ	Mean (P_m)	COV (V_P)	β
ANSI/AISC 360-16	0.9	0.976	0.056	2.533
Modified ANSI/AISC 360-16	0.9	1.042	0.062	2.799
ASCE/SEI 48-19	0.9	0.875	0.082	1.978
Modified ASCE/SEI 48-19	0.9	1.040	0.064	2.790

Table 8. Summary of statistical parameters.

Design method	Steel grade	$f_{y,m}/f_{y,n}$	V_{fy}	V_A	V_E
prEN 1993-1-1:2020	355	1.20	0.050	0.026	0.03
	460	1.15	0.045	0.026	0.03
	690	1.10	0.035	0.026	0.03
ANSI/AISC 360-16	All	1.10	0.100	-	0.05